

Spin anisotropy due to spin-orbit coupling in optimally hole-doped $\text{Ba}_{0.67}\text{K}_{0.33}\text{Fe}_2\text{As}_2$

Yu Song,^{1,*} Haoran Man,¹ Rui Zhang,¹ Xingye Lu,¹ Chenglin Zhang,¹ Meng Wang,² Guotai Tan,³ L.-P. Regnault,^{4,5} Yixi Su,⁶ Jian Kang,⁷ Rafael M. Fernandes,⁷ and Pengcheng Dai^{1,3,†}

¹*Department of Physics and Astronomy, Rice University, Houston, Texas 77005, USA*

²*Department of Physics, University of California, Berkeley, California 94720, USA*

³*Center for Advanced Quantum Studies and Department of Physics, Beijing Normal University, Beijing 100875, China*

⁴*Université Grenoble Alpes, 38042 Grenoble, France*

⁵*CEA-Grenoble, INAC-MEM-MDN, 38054 Grenoble, France*

⁶*Jülich Centre for Neutron Science, Forschungszentrum Jülich GmbH, Outstation at MLZ, D-85747 Garching, Germany*

⁷*School of Physics and Astronomy, University of Minnesota, Minneapolis, Minnesota 55455, USA*

We use polarized inelastic neutron scattering to study the temperature and energy dependence of spin space anisotropies in the optimally hole-doped iron pnictide $\text{Ba}_{0.67}\text{K}_{0.33}\text{Fe}_2\text{As}_2$ ($T_c = 38$ K). In the superconducting state, while the high-energy part of the magnetic spectrum is nearly isotropic, the low-energy part displays a pronounced anisotropy, manifested by a c -axis polarized resonance. We also observe that the spin anisotropy in superconducting $\text{Ba}_{0.67}\text{K}_{0.33}\text{Fe}_2\text{As}_2$ extends to higher energies compared to electron-doped $\text{BaFe}_{2-x}\text{TM}_x\text{As}_2$ ($\text{TM} = \text{Co, Ni}$) and isovalent-doped $\text{BaFe}_2\text{As}_{1.4}\text{P}_{0.6}$, suggesting a connection between T_c and the energy scale of the spin anisotropy. In the normal state, the low-energy spin anisotropy for optimally hole- and electron-doped iron pnictides onset at temperatures similar to the temperatures at which the elasto-resistance deviate from Curie-Weiss behavior, pointing to a possible connection between the two phenomena. Our results highlight the relevance of the spin-orbit coupling to the superconductivity of the iron pnictides.

PACS numbers: 74.25.Ha, 74.70.-b, 78.70.Nx

I. INTRODUCTION

The parent compounds of iron pnictide superconductors, such as LaFeAsO and BaFe_2As_2 , form stripe antiferromagnetic (AF) order at T_N below a tetragonal-to-orthorhombic structural transition temperature T_S [inset in Fig. 1(b)]¹⁻⁴. Superconductivity can be induced by partially replacing Ba by K in BaFe_2As_2 to form hole-doped $\text{Ba}_{1-x}\text{K}_x\text{Fe}_2\text{As}_2$ ⁵⁻⁹ or by partially replacing Fe by TM ($\text{TM} = \text{Co, Ni}$) to form electron-doped $\text{BaFe}_{2-x}\text{TM}_x\text{As}_2$ ¹⁰⁻¹³. Importantly, the resulting phase diagrams exhibit significant asymmetry between electron- and hole-doping [Figs. 1(a) and 1(b)]^{3,4}. For instance, while near optimal doping the stripe AF order becomes incommensurate for electron-doped $\text{BaFe}_{2-x}\text{TM}_x\text{As}_2$ ^{10,11} [see arrow in Fig. 1(b)], a double- \mathbf{Q} tetragonal magnetic structure with ordered moments along the c -axis is observed in hole-doped $\text{Ba}_{1-x}\text{K}_x\text{Fe}_2\text{As}_2$ [see region of the phase diagram near the arrow in Fig. 1(a)]⁶⁻⁹.

Nevertheless, upon entering the superconducting state, a magnetic resonance mode appears in the magnetic spectrum in both cases at the AF wave vector (\mathbf{Q}_{AF})¹⁴⁻¹⁷. Furthermore, by measuring the splitting of the electronic states at high-symmetry points in reciprocal space¹⁸, angle-resolved photoemission spectroscopy (ARPES) measurements find that spin-orbit coupling (SOC) is present in both electron- and hole-doped iron pnictides with a similar energy scale ~ 10 meV¹⁹. Also common to both optimally electron-doped $\text{BaFe}_{2-x}\text{TM}_x\text{As}_2$ ^{20,21} and hole-doped $\text{Ba}_{1-x}\text{K}_x\text{Fe}_2\text{As}_2$ ^{22,23} is the presence of

electronic nematic fluctuations, as revealed by the elasto-resistance – i.e. the rate of change of the resistivity anisotropy with respect to applied in-plane uniaxial strain [Fig. 1(c)]²⁴. The elasto-resistance diverges with a Curie-Weiss form for both classes of materials as well as for isovalent-doped $\text{BaFe}_2\text{As}_{1.4}\text{P}_{0.6}$ ²⁵. Deviation from the Curie-Weiss behavior is seen in both optimally electron- and hole-doped BaFe_2As_2 at low temperatures, while no deviation is seen in $\text{BaFe}_2\text{As}_{1.4}\text{P}_{0.6}$ down to T_c [Fig. 1(d)]²⁵.

In addition to its impact on the electronic spectrum^{19,26}, SOC also converts crystalline anisotropies into anisotropies in spin space, as seen from nuclear magnetic resonance studies²⁷. The spin anisotropy resulting from SOC plays an essential role for the double- \mathbf{Q} magnetic phase⁶⁻⁹, in which the ordered moments align along the c -axis²⁸. If SOC was absent, the spin excitations in the paramagnetic tetragonal state of the iron pnictides would be isotropic in spin space [Fig. 1(e)]. However, due to the presence of a sizable SOC, an anisotropy is developed in the spin excitations, which can be quantitatively determined by neutron polarization analysis²⁹. In the antiferromagnetically ordered phases of the parent compounds BaFe_2As_2 and NaFeAs ^{30,31}, where the ordered moments point parallel to the orthorhombic a -axis [inset in Fig. 1(b)], spin waves exhibit significant anisotropy, with c -axis polarized spin waves occurring at lower energy compared to b -axis polarized spin waves³²⁻³⁴. To elucidate the relevance of SOC to superconductivity, it is instructive to compare the behavior of the spin anisotropy in hole-doped and

electron-doped BaFe_2As_2 , since the maximum values of T_c are quite different in these two cases – $T_c \approx 38$ K for optimally hole-doped $\text{Ba}_{0.67}\text{K}_{0.33}\text{Fe}_2\text{As}_2$ and $T_c \approx 25$ K for optimally electron-doped $\text{BaFe}_{1.86}\text{Co}_{0.14}\text{As}_2$. Previous analysis of the electron-doped case revealed that the spin anisotropy persists in the paramagnetic tetragonal phase for doping levels up to or slightly beyond optimal doping^{35–40}, but vanishes in the well-overdoped regime^{39,41}.

In this paper, we present polarized neutron scattering studies of spin excitations in optimally hole-doped $\text{Ba}_{0.67}\text{K}_{0.33}\text{Fe}_2\text{As}_2$ ^{17,38}. In the normal state, we find that the spin anisotropy of $\text{Ba}_{0.67}\text{K}_{0.33}\text{Fe}_2\text{As}_2$ persists to ~ 100 K for $E = 3$ meV, similarly to the case of near-optimally electron-doped $\text{BaFe}_{2-x}\text{TM}_x\text{As}_2$, where spin anisotropy at $\mathbf{Q}_{\text{AF}} = (1, 0, 1)$ was found below $E \approx 7$ meV and up to ~ 70 K^{36,37}. We associate the onset of normal state spin anisotropy with the nematic susceptibility deviating from Curie-Weiss behavior measured via elastoresistance [see vertical arrows in Fig. 1(d)]²⁵, indicating an important role of spin excitations in transport properties of iron pnictides.

Upon entering the superconducting state, we find that while at high energies ($E \geq 14$ meV) the spectrum is nearly isotropic as found in previous work³⁸, at low energies the resonance mode is strongly anisotropic, being dominated by a c -axis polarized component. We attribute this behavior to the fact that the superconducting state is close to the double- \mathbf{Q} magnetic phase, in which the magnetic moments point out-of-plane^{7,8}. Indeed, by adding a spin-anisotropic term that favors c -axis spin orientation in a simple two-band theoretical model, we find that the resonance mode in the c -axis polarized channel has in general a lower energy than in other channels, and that this energy difference increases as the magnetically ordered state is approached. Our analysis also reveals an interesting correlation between the energy scale of the spin anisotropy in the superconducting state and T_c ^{35–40,42}, suggesting that SOC is an integral part of the superconductivity of iron pnictides.

II. EXPERIMENTAL RESULTS

Polarized inelastic neutron scattering measurements were carried out using the IN22 triple-axis spectrometer at Institut Laue-Langevin, Grenoble, France. We studied $\text{Ba}_{0.67}\text{K}_{0.33}\text{Fe}_2\text{As}_2$ single crystals ($a = b \approx 5.56$ Å, $c = 13.29$ Å) co-aligned in the $[H, 0, L]$ scattering plane used in previous works^{38,44}. We use the orthorhombic notation suitable for AF ordered iron pnictides even though $\text{Ba}_{0.67}\text{K}_{0.33}\text{Fe}_2\text{As}_2$ has a tetragonal structure and is paramagnetic at all temperatures^{17,38}. Thus, the momentum transfer is $\mathbf{Q} = H\mathbf{a}^* + K\mathbf{b}^* + L\mathbf{c}^*$, with $\mathbf{a}^* = \frac{2\pi}{a}\hat{\mathbf{a}}$, $\mathbf{b}^* = \frac{2\pi}{b}\hat{\mathbf{b}}$ and $\mathbf{c}^* = \frac{2\pi}{c}\hat{\mathbf{c}}$, where H , K and L are Miller indices. In this notation, magnetic order in BaFe_2As_2 occurs at $\mathbf{Q}_{\text{AF}} = (1, 0, L)$ with $L = 1, 3, 5, \dots$ [Fig. 1(e)]. Three neutron spin-flip (SF) cross sections σ_x^{SF} , σ_y^{SF} and

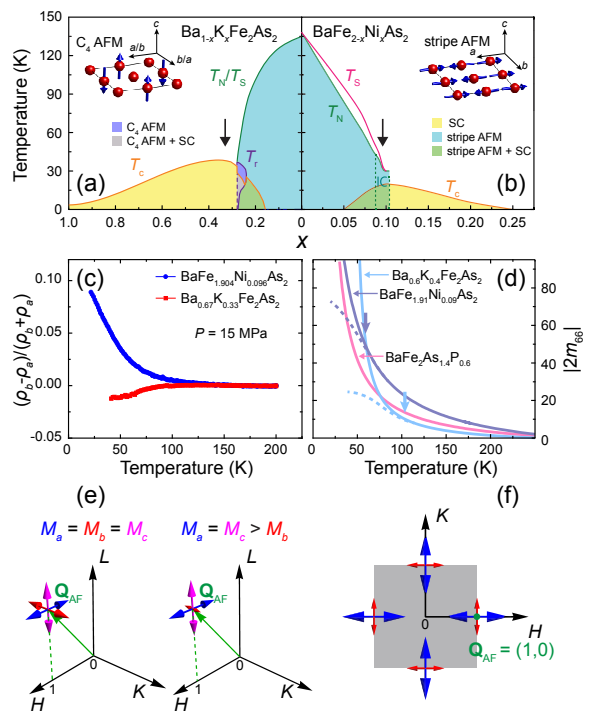


Figure 1: (Color online) The electronic phase diagrams of (a) hole- and (b) electron-doped BaFe_2As_2 . While parent compounds of iron pnictides have stripe AF order [inset in (b)]², the tetragonal double- \mathbf{Q} C_4 AF order is found in hole-doped BaFe_2As_2 near optimal superconductivity [inset in (a)]^{6–9}. T_S , T_N , T_c and T_T mark the tetragonal-to-orthorhombic structural transition, the paramagnetic-to-AF transition, the superconducting transition and the transition into the C_4 magnetic phase. The phase diagrams in (a) and (b) are adapted from Refs.⁵⁷ and⁴. (c) Resistivity anisotropy $(\rho_a - \rho_b)/(\rho_a + \rho_b)$ of $\text{BaFe}_{1.904}\text{Ni}_{0.096}\text{As}_2$ and $\text{Ba}_{0.67}\text{K}_{0.33}\text{Fe}_2\text{As}_2$ under uniaxial pressure of $P = 15$ MPa measured using a mechanical clamp that can vary applied pressure *in-situ*⁴³. (d) Elastoresistance $|2m_{66}|$ for optimally-doped $\text{BaFe}_{1.91}\text{Ni}_{0.09}\text{As}_2$, $\text{Ba}_{0.6}\text{K}_{0.4}\text{Fe}_2\text{As}_2$, and $\text{BaFe}_2\text{As}_{1.4}\text{P}_{0.6}$, adapted from Ref.²⁵. The solid lines are Curie-Weiss fits to the data and dashed lines represent deviations from the Curie-Weiss form. Vertical arrows mark the temperature at which such deviations begin. (e) Schematic of isotropic spin excitations (left) and anisotropic spin excitations (right), with the sizes of arrows centered at \mathbf{Q}_{AF} representing the intensities of spin excitations polarized along different directions. (f) In-plane spin anisotropy discussed in this work (represented by red and blue arrows of different sizes) preserves four-fold rotational symmetry of the tetragonal unit cell because \mathbf{Q}_{AF} is at an edge of the Brillouin zone of the unfolded tetragonal (i.e. 1-Fe) unit cell⁴⁶, depicted by the shaded gray area.

σ_z^{SF} were measured, with the usual convention $x \parallel \mathbf{Q}$, $y \perp \mathbf{Q}$ and in the scattering plane, and z perpendicular to the scattering plane. Magnetic neutron scattering directly measures the magnetic scattering function $S^{\alpha\beta}(\mathbf{Q}, E)$, which is proportional to the imaginary part of the dynamic susceptibility through the Bose factor, $S^{\alpha\beta}(\mathbf{Q}, E) \propto [1 - \exp(-\frac{E}{k_B T})]^{-1} \text{Im} \chi^{\alpha\beta}(\mathbf{Q}, E)$ ⁴⁵. Follow-

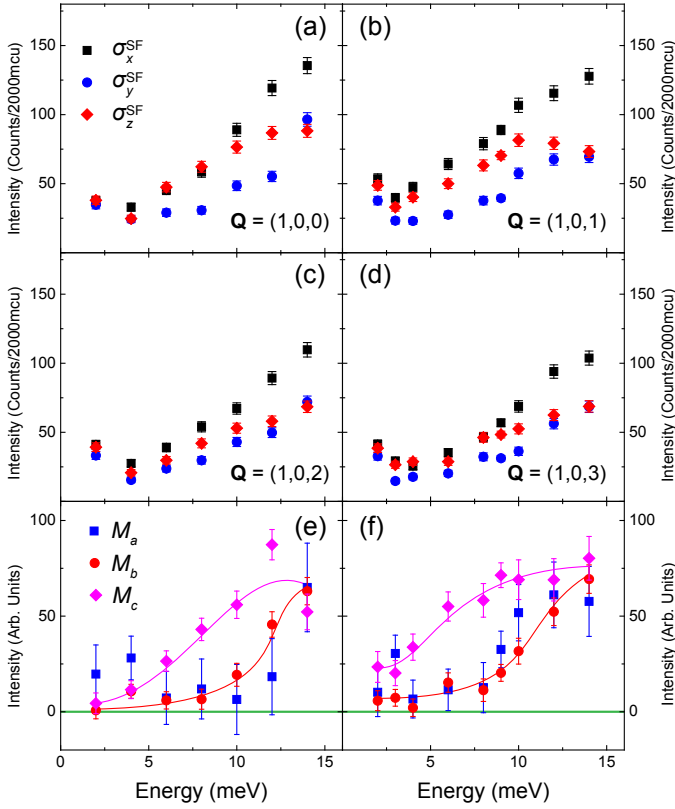


Figure 2: (Color online) Constant- \mathbf{Q} scans of σ_x^{SF} , σ_y^{SF} and σ_z^{SF} at $\mathbf{Q} = (1,0,L)$ for (a) $L = 0$, (b) $L = 1$, (c) $L = 2$ and (d) $L = 3$ measured at 2 K. Using the measured cross sections in (a) - (d), M_a , M_b and M_c are obtained for (e) even and (f) odd L . The solid lines are guides to the eye.

ing earlier works^{34,36,38,39,41}, we denote the diagonal components of the magnetic scattering function $S^{\alpha\alpha}$ as M_α . M_y and M_z can be obtained from measured SF cross sections through $\sigma_x^{\text{SF}} - \sigma_y^{\text{SF}} \propto M_y$ and $\sigma_x^{\text{SF}} - \sigma_z^{\text{SF}} \propto M_z$. M_y and M_z are related to $M_a = M_{100}$, $M_b = M_{010}$ and $M_c = M_{001}$ through $M_y = \sin^2\theta M_a + \cos^2\theta M_c$ and $M_z = M_b$ ^{34,36,38,39,41}, with θ being the angle between \mathbf{Q} and \mathbf{a}^*/a . Anisotropy between M_a and M_b at \mathbf{Q}_{AF} is allowed in the paramagnetic tetragonal state of iron pnictides and does not break four-fold rotation symmetry of the lattice because \mathbf{Q}_{AF} is at an edge of the Brillouin zone of the unfolded tetragonal (1-Fe) unit cell⁴⁶, as depicted in Fig. 1(f). Another manifestation of the lack of four-fold rotational symmetry for magnetic excitations at \mathbf{Q}_{AF} is the anisotropic in-plane correlation lengths seen in the paramagnetic tetragonal states of BaFe_2As_2 ⁴⁷ and CaFe_2As_2 ⁴⁸. By obtaining M_y and M_z at two equivalent wave vectors with different θ , it is then possible to obtain M_a , M_b , and M_c ^{33,34,36,39}.

Figure 2 summarizes constant- \mathbf{Q} scans at 2 K and $\mathbf{Q} = (1,0,L)$ with $L = 0, 1, 2$ and 3. From Fig. 2(a)-(d), it is clear that $\sigma_x^{\text{SF}} > \sigma_z^{\text{SF}} \geq \sigma_y^{\text{SF}}$ below $E \approx 14$ meV, meaning that spin anisotropy exists below this energy while excitations above this energy are isotropic as

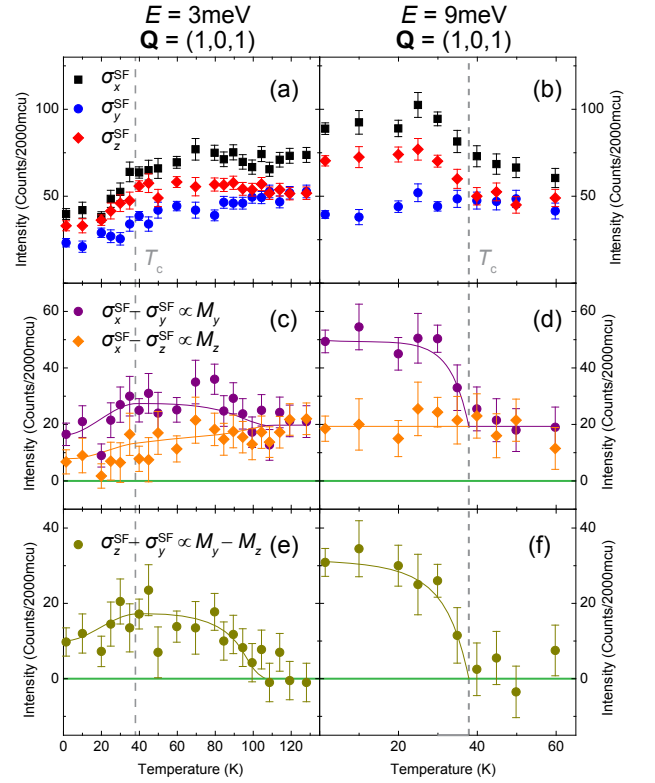


Figure 3: (Color online) Temperature scans of σ_x^{SF} , σ_y^{SF} and σ_z^{SF} at $\mathbf{Q} = (1,0,1)$ with (a) $E = 3$ meV and (b) $E = 9$ meV. The differences $\sigma_x^{\text{SF}} - \sigma_y^{\text{SF}}$ and $\sigma_x^{\text{SF}} - \sigma_z^{\text{SF}}$ which are respectively proportional to M_y and M_z are shown for (c) $E = 3$ meV and (d) $E = 9$ meV. The differences $\sigma_z^{\text{SF}} - \sigma_y^{\text{SF}}$ which is proportional to $M_y - M_z$ are shown for (e) $E = 3$ meV and (f) $E = 9$ meV. The solid lines are guides to the eye. The dashed vertical lines mark T_c .

shown in previous work³⁸. Although magnetic order is fully suppressed in $\text{Ba}_{0.67}\text{K}_{0.33}\text{Fe}_2\text{As}_2$, the spin gap E_g in the superconducting state displays strong L dependence, with $E_g \approx 0.75$ meV for odd L and $E_g \approx 5$ meV for even L ^{17,38}. From Figs. 2 (b) and 2(d), we observe that the small gap for odd L is due to M_y , with $\sigma_x^{\text{SF}} \approx \sigma_z^{\text{SF}} > \sigma_y^{\text{SF}}$ for $E \lesssim 5$ meV. Magnetic excitations are gapped in the same energy range for even L as can be seen in Figs. 2(a) and 2(c), with $\sigma_x^{\text{SF}} \approx \sigma_y^{\text{SF}} \approx \sigma_z^{\text{SF}}$. M_a , M_b and M_c for even and odd L are shown in Figs. 2 (e) and (f), respectively. While M_b is weakly L -dependent, M_c clearly displays different behaviors for even and odd L . Because in the energy range $5 \lesssim E \lesssim 10$ meV M_c dominates and is dispersive along L , we uniquely identify it with the anisotropic resonance that disperses along L which was previously observed in the same sample³⁸.

To gain further insight into the spin anisotropy of $\text{Ba}_{0.67}\text{K}_{0.33}\text{Fe}_2\text{As}_2$, we carried out temperature scans at $\mathbf{Q}_{\text{AF}} = (1,0,1)$ for $E = 3$ meV and $E = 9$ meV, as shown in Figs. 3(a) and 3(b). At $E = 3$ meV, the spin anisotropy with $\sigma_z^{\text{SF}} > \sigma_y^{\text{SF}}$ persists up to ~ 100 K. Although below T_c the magnetic signal is suppressed in all

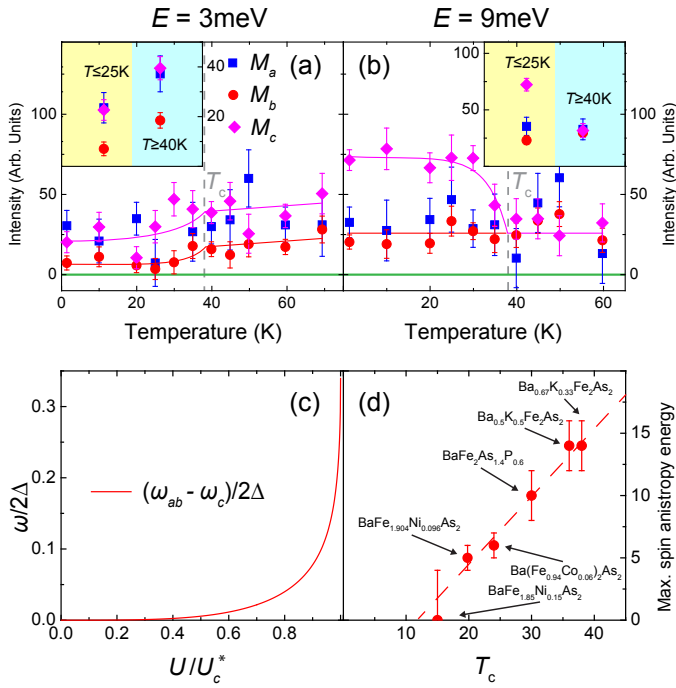


Figure 4: (Color online) Temperature dependence of M_a , M_b and M_c for (a) $E = 3$ meV and (b) $E = 9$ meV. The solid lines are guides to the eye and dashed vertical lines mark T_c . The insets in (a) and (b) show binned M_a , M_b and M_c from (a) and (b) for $T \leq 25$ K and $T \geq 38$ K. The insets share the same y -axis label as (a) and (b). (c) Difference between the energies of the ab -polarized and the c -polarized resonance modes obtained in our theoretical model. U is the electronic interaction that triggers long-range magnetic order with the moments pointing along the c -axis when $U = U_c^*$. (d) Maximum energy at which spin anisotropy is observed in the superconducting state of several doped BaFe_2As_2 compounds. Results are obtained from Refs.^{36–38,40–42}. For overdoped $\text{BaFe}_{1.85}\text{Ni}_{0.15}\text{As}_2$ the excitations are isotropic but low energy excitations are gapped below $E \approx 4$ meV⁴¹, therefore for this compound we assign the maximum spin anisotropy energy to be 0, but with an uncertainty of 4 meV.

three SF cross sections, the normal-state anisotropy persists [Fig. 3(a)]. At $E = 9$ meV, the spin anisotropy disappears above T_c , suggesting that the main contribution to the spin anisotropy in the superconducting state arises from the anisotropic resonance mode³⁸. In Figs. 3(c) and 3(d), $\sigma_x^{\text{SF}} - \sigma_y^{\text{SF}} \propto M_y$ and $\sigma_x^{\text{SF}} - \sigma_z^{\text{SF}} \propto M_z$ are shown. At $E = 3$ meV, $M_y > M_z$ for $T \lesssim 100$ K and both are suppressed below T_c . At $E = 9$ meV, while a clear resonance mode with an order-parameter-like temperature dependence is seen in M_y , M_z remains constant across T_c . The temperature onset of spin anisotropy is more clearly seen in Fig. 3(e) and (f), which plots $\sigma_z^{\text{SF}} - \sigma_y^{\text{SF}} \propto M_y - M_z$ for $E = 3$ meV and $E = 9$ meV, respectively.

To obtain the temperature dependence of M_a , M_b and M_c , we measured σ_x^{SF} , σ_y^{SF} and σ_z^{SF} at $\mathbf{Q}_{\text{AF}} = (1, 0, 3)$ for $E = 3$ meV and $E = 9$ meV⁴³. Combining the temperature dependence for $L = 1$ and $L = 3$, M_a , M_b and M_c

are obtained for odd L as shown in Fig. 4(a) and 4(b). At $E = 3$ meV, $M_a \approx M_c > M_b$ within the probed temperature range, and all three channels decrease in intensity below T_c . At $E = 9$ meV, M_a and M_b display a weak temperature dependence while M_c is sharply affected by T_c . To corroborate our conclusion, we binned data points in Fig. 4(a) and 4(b) that are well below T_c ($T \leq 25$ K) and above T_c ($T \geq 40$ K), as shown in the insets of Figs. 4(a) and 4(b). While magnetic excitations at $E = 3$ meV are suppressed upon entering the superconducting state, the polarization of these magnetic excitations seems to remain the same, persisting up to $T \approx 100$ K. On the other hand, at $E = 9$ meV, magnetic excitations are nearly isotropic above T_c , while $M_c > M_a \approx M_b$ well below T_c . Therefore, the c -axis polarized anisotropic resonance is directly coupled to superconductivity with an order-parameter-like temperature dependence.

III. DISCUSSION AND CONCLUSION

To understand the origin of this c -axis polarized spin resonance, we consider a simple two band model⁴³ in which the resonance mode arises due to the sign change of the gap function between a hole pocket and an electron pocket displaced from each other by the AF ordering vector \mathbf{Q}_{AF} ^{49–51}. Without SOC, the energy of the resonance mode is the same for all polarizations, being close to 2Δ far from the putative magnetic quantum phase transition inside the superconducting dome [$U \ll U_c^*$ in Fig. 4(c)], but vanishing as the transition is approached [$U \rightarrow U_c^*$ in Fig. 4(c)]. SOC, however, promotes a spin anisotropy term that makes the magnetic moments point along the c -axis for hole-doped compounds²⁸. As a result, the energy of the resonance mode polarized along the c -axis is suppressed much faster as the magnetic transition is approached, yielding $\omega_c < \omega_{ab}$ [Fig. 4(c)]. This behavior is in qualitative agreement with our experimental results, with the resonance seen in M_c indeed at lower energies. It should also be noted that our model does not capture the broadening of the resonance, which is rather pronounced in the experimental data. Our simple model has two additional consequences: first, as the system is overdoped and moves farther from the magnetically ordered state, the resonance mode should become more isotropic. While spin anisotropy persists in slightly overdoped $\text{Ba}_{0.5}\text{K}_{0.5}\text{Fe}_2\text{As}_2$ ($T_c = 36$ K)⁴⁰, how it evolves in K-well-overdoped samples remains to be seen. Furthermore, because in electron-doped compounds the moments point along the a direction, the resonance is expected to be polarized along the a -axis. Although this is the case in electron-doped $\text{NaFe}_{0.985}\text{Co}_{0.015}\text{As}$ ³⁹, the sample studied had long-range AF order. For electron-doped $\text{Ba}(\text{Fe}_{0.94}\text{Co}_{0.06})_2\text{As}_2$ ³⁷, the anisotropic resonance was argued to be also polarized along c -axis, based on the assumption $M_a = M_b$ and the observation $M_y > M_z = 0$ for the anisotropic resonance. As we have shown here and in previous work³⁶, even in the tetragonal state M_a and

M_b are not necessarily the same and it is unclear whether there is also significant resonance spectral weight polarized along the a -axis in previous work³⁷. Spin anisotropy of spin excitations has also been detected in the superconducting states of LiFeAs⁵² and FeSe_{0.5}Te_{0.5}⁵³, consistent with significant spin-orbit coupling detected by ARPES^{19,26} in these systems.

The normal state spin anisotropy at low energies persists to a temperature significantly higher than T_c [~ 70 K in BaFe_{1.094}Ni_{0.096}As₂³⁶ and ~ 100 K in Ba_{0.67}K_{0.33}Fe₂As₂, Fig. 3(e)] for both electron- and hole-doped BaFe₂As₂ near optimal doping. The temperature at which spin anisotropy onsets is similar to the temperature at which the nematic susceptibility deviates from Curie-Weiss behavior²⁵, suggesting a common origin for both phenomena [Fig. 1(d)]. For optimally-doped BaFe₂As_{1.4}P_{0.6}, whose nematic susceptibility shows no deviation from the Curie-Weiss form [Fig. 1(d)]²⁵, no spin anisotropy is observed right above T_c ⁴². While disorder is likely to play an important role in explaining this deviation from Curie-Weiss behavior in the elastoresistance²⁵, our results suggest that the spin anisotropy may also be important. Indeed, previous INS experiments revealed the intimate relationship between nematicity and magnetic fluctuations^{54–56}. Theoretically, the nematic susceptibility increases with increasing magnetic fluctuations in all polarization channels²⁴. However, once a spin anisotropy sets in, fluctuations re-

lated to the spin components perpendicular to the easy axis increase more slowly with decreasing temperature. As a result, the nematic susceptibility should also increase more slowly, which may contribute to the deviation from Curie-Weiss behavior observed experimentally.

Finally, the maximum energies at which spin anisotropy is observed in the superconducting states of several doped BaFe₂As₂ compounds are plotted as function of T_c in Fig. 4(d). Note that the spin anisotropy of the resonance in the superconducting state is also present in BaFe₂As_{1.4}P_{0.6}, despite the absence of spin anisotropy in the normal state⁴². We note a clear positive correlation between the energy scale of the spin anisotropy and T_c , suggesting SOC to be an important ingredient for understanding superconductivity in iron pnictides.

IV. ACKNOWLEDGMENTS

We thank Ilya Eremin, Qimiao Si, and Jiangping Hu for useful discussions. The neutron work at Rice is supported by the U.S. NSF-DMR-1362219 and DMR-1436006 (P.D.). This work is also supported by the Robert A. Welch Foundation Grant Nos. C-1839 (P.D.). Work performed by R.M.F. and J.K. is supported by the U.S. Department of Energy, Office of Science, Basic Energy Sciences, under Award number de-sc0012336.

* Electronic address: Yu.Song@rice.edu

† Electronic address: pdai@rice.edu

¹ Y. Kamihara, T. Watanabe, M. Hirano, and H. Hosono, *J. Am. Chem. Soc.* **130**, 3296 (2008).

² C. de la Cruz, Q. Huang, J. W. Lynn, J. Li, W. Ratcliff II, J. L. Zarestky, H. A. Mook, G. F. Chen, J. L. Luo, N. L. Wang, and P. C. Dai, *Nature* **453**, 899 (2008).

³ D. C. Johnston, *Advances in Physics* **59**, 803 (2010).

⁴ P. C. Dai, *Rev. Mod. Phys.* **87**, 855 (2015).

⁵ Marianne Rotter, Marcus Tegel, and Dirk Johrendt, *Phys. Rev. Lett.* **101**, 107006 (2008).

⁶ S. Avci, O. Chmaissem, J.M. Allred, S. Rosenkranz, I. Eremin, A.V. Chubukov, D.E. Bugaris, D.Y. Chung, M.G. Kanatzidis, J.-P. Castellan, J.A. Schlueter, H. Claus, D.D. Khalyavin, P. Manuel, A. Daoud-Aladine, and R. Osborn, *Nat. Commun.* **5**, 3845 (2014).

⁷ F. Waßer, A. Schneidewind, Y. Sidis, S. Wurmehl, S. Aswartham, B. Büchner, and M. Braden, *Phys. Rev. B* **91**, 060505 (2015).

⁸ J. M. Allred, K. M. Taddei, D. E. Bugaris, M. J. Krogstad, S. H. Lapidus, D. Y. Chung, H. Claus, M. G. Kanatzidis, D. E. Brown, J. Kang, R. M. Fernandes, I. Eremin, S. Rosenkranz, O. Chmaissem, and R. Osborn, *Nat. Phys.* **12**, 493 (2016).

⁹ J. M. Allred, S. Avci, D. Y. Chung, H. Claus, D. D. Khalyavin, P. Manuel, K. M. Taddei, M. G. Kanatzidis, S. Rosenkranz, R. Osborn, and O. Chmaissem, *Phys. Rev. B* **92**, 094515 (2015).

¹⁰ D. K. Pratt, M. G. Kim, A. Kreyssig, Y. B. Lee, G. S.

Tucker, A. Thaler, W. Tian, J. L. Zarestky, S. L. Bud'ko, P. C. Canfield, B. N. Harmon, A. I. Goldman, and R. J. McQueeney, *Phys. Rev. Lett.* **106**, 257001 (2011).

¹¹ Xingye Lu, H. Gretarsson, Rui Zhang, Xuerong Liu, Huiqian Luo, Wei Tian, Mark Laver, Z. Yamani, Young-June Kim, A. H. Nevidomskyy, Qimiao Si, and Pengcheng Dai, *Phys. Rev. Lett.* **110**, 257001 (2013).

¹² Athena S. Sefat, Rongying Jin, Michael A. McGuire, Brian C. Sales, David J. Singh, and David Mandrus, *Phys. Rev. Lett.* **101**, 117004 (2008).

¹³ L. J. Li, Y. K. Luo, Q. B. Wang, H. Chen, Z. Ren, Q. Tao, Y. K. Li, X. Lin, M. He, Z.W. Zhu, G. H. Cao, and Z. A. Xu, *New J. Phys.* **11**, 025008 (2009).

¹⁴ A. D. Christianson *et al.*, *Nature* **456**, 930-932 (2008).

¹⁵ M. D. Lumsden, A. D. Christianson, D. Parshall, M. B. Stone, S. E. Nagler, G. J. MacDougall, H. A. Mook, K. Lokshin, T. Egami, D. L. Abernathy, E. A. Goremychkin, R. Osborn, M. A. McGuire, A. S. Sefat, R. Jin, B. C. Sales, and D. Mandrus, *Phys. Rev. Lett.* **102**, 107005 (2009).

¹⁶ Songxue Chi, Astrid Schneidewind, Jun Zhao, Leland W. Harriger, Linjun Li, Yongkang Luo, Guanghan Cao, Zhu'an Xu, Micheal Loewenhaupt, Jiangping Hu, and Pengcheng Dai, *Phys. Rev. Lett.* **102**, 107006 (2009).

¹⁷ Chenglin Zhang, Meng Wang, Huiqian Luo, Miaoyin Wang, Mengshu Liu, Jun Zhao, D. L. Abernathy, T. A. Maier, Karol Marty, M. D. Lumsden, Songxue Chi, Sung Chang, Jose A. Rodriguez-Rivera, J. W. Lynn, Tao Xiang, Jiangping Hu, and Pengcheng Dai, *Sci. Rep.* **1**, 115 (2011).

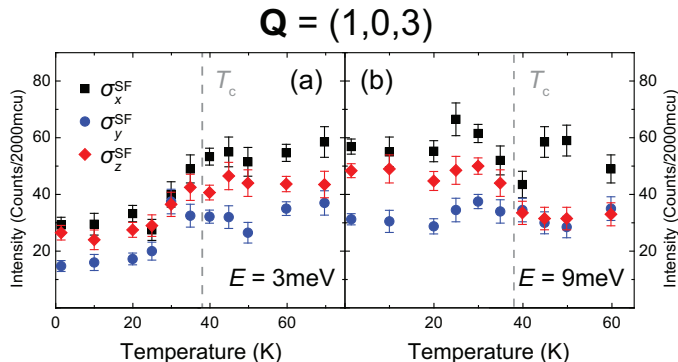
¹⁸ R. M. Fernandes and O. Vafek, *Phys. Rev. B* **90**, 214514

- (2014).
- 19 S. V. Borisenko, D. V. Evtushinsky, Z.-H. Liu, I. Morozov, R. Kappenberger, S. Wurmehl, B. Büchner, A. N. Yaresko, T. K. Kim, M. Hoesch, T. Wolf, and N. D. Zhigadlo, *Nat. Phys.* **12**, 311 (2016).
 - 20 J. H. Chu, J. G. Analytis, K. De Greve, P. L. McMahon, Z. Islam, Y. Yamamoto, and I. R. Fisher, *Science* **329**, 824 (2010).
 - 21 X. Y. Lu, K.-F. Tseng, T. Keller, W. L. Zhang, D. Hu, Y. Song, H. R. Man, J. T. Park, H. Q. Luo, S. L. Li, A. H. Nevidomskyy, and Pengcheng Dai, *Phys. Rev. B* **93**, 134519 (2016).
 - 22 J. J. Ying, X. F. Wang, T. Wu, Z. J. Xiang, R. H. Liu, Y. J. Yan, A. F. Wang, M. Zhang, G. J. Ye, P. Cheng, J. P. Hu, and X. H. Chen, *Phys. Rev. Lett.* **107**, 067001 (2011).
 - 23 E. C. Blomberg, M. A. Tanatar, R. M. Fernandes, I. I. Mazin, Bing Shen, Hai-Hu Wen, M. D. Johannes, J. Schmalian, and R. Prozorov, *Nat. Commun.* **4**, 1914 (2013).
 - 24 R. M. Fernandes, A. V. Chubukov, and J. Schmalian, *Nat. Phys.* **10**, 97 (2014).
 - 25 Hsueh-Hui Kuo, Jiun-Haw Chu, Johanna C. Palmstrom, Steven A. Kivelson, Ian R. Fisher, *Science* **352**, 958 (2016).
 - 26 P. D. Johnson, H.-B. Yang, J. D. Rameau, G. D. Gu, Z.-H. Pan, T. Valla, M. Weinert, and A. V. Fedorov, *Phys. Rev. Lett.* **114**, 167001 (2015).
 - 27 Z. Li, D. L. Sun, C. T. Lin, Y. H. Su, J. P. Hu, and Guoqing Zheng, *Phys. Rev. B* **83**, 140506 (2011).
 - 28 Morten H. Christensen, Jian Kang, Brian M. Andersen, Ilya Eremin, and Rafael M. Fernandes, *Phys. Rev. B* **92**, 214509 (2015).
 - 29 R. M. Moon, T. Riste, and W. C. Koehler, *Phys. Rev.* **181**, 920 (1969).
 - 30 Q. Huang, Y. Qiu, Wei Bao, M. A. Green, J. W. Lynn, Y. C. Gasparovic, T. Wu, G. Wu, and X. H. Chen, *Phys. Rev. Lett.* **101**, 257003 (2008).
 - 31 S. L. Li, C. de la Cruz, Q. Huang, G. F. Chen, T.-L. Xia, J. L. Luo, N. L. Wang, and P. C. Dai, *Phys. Rev. B* **80**, 020504(R) (2009).
 - 32 N. Qureshi, P. Steffens, S. Wurmehl, S. Aswartham, B. Büchner, and M. Braden, *Phys. Rev. B* **86**, 060410 (2012).
 - 33 Chong Wang, Rui Zhang, Fa Wang, Huiqian Luo, L. P. Regnault, Pengcheng Dai, and Yuan Li, *Phys. Rev. X* **3**, 041036 (2013).
 - 34 Yu Song, Louis-Pierre Regnault, Chenglin Zhang, Guotai Tan, Scott V. Carr, Songxue Chi, A. D. Christianson, Tao Xiang, and Pengcheng Dai, *Phys. Rev. B* **88**, 134512 (2013).
 - 35 O. J. Lipscombe, Leland W. Harriger, P. G. Freeman, M. Enderle, Chenglin Zhang, Miaoying Wang, Takeshi Egami, Jiangping Hu, Tao Xiang, M. R. Norman, and Pengcheng Dai, *Phys. Rev. B* **82**, 064515 (2010).
 - 36 Huiqian Luo, Meng Wang, Chenglin Zhang, Xingye Lu, Louis-Pierre Regnault, Rui Zhang, Shiliang Li, Jiangping Hu, and Pengcheng Dai, *Phys. Rev. Lett.* **111**, 107006 (2013).
 - 37 P. Steffens, C. H. Lee, N. Qureshi, K. Kihou, A. Iyo, H. Eisaki, and M. Braden, *Phys. Rev. Lett.* **110**, 137001 (2013).
 - 38 Chenglin Zhang, Mengshu Liu, Yixi Su, Louis-Pierre Regnault, Meng Wang, Guotai Tan, Th. Brückel, Takeshi Egami, and Pengcheng Dai, *Phys. Rev. B* **87**, 081101 (2013).
 - 39 Chenglin Zhang, Yu Song, L.-P. Regnault, Yixi Su, M. Enderle, J. Kulda, Guotai Tan, Zachary C. Sims, Takeshi Egami, Qimiao Si, and Pengcheng Dai, *Phys. Rev. B* **90**, 140502 (2014).
 - 40 N. Qureshi, C. H. Lee, K. Kihou, K. Schmalzl, P. Steffens, and M. Braden, *Phys. Rev. B* **90**, 100502 (2014).
 - 41 Mengshu Liu, C. Lester, Jiri Kulda, Xinye Lu, Huiqian Luo, Meng Wang, S. M. Hayden, and Pengcheng Dai, *Phys. Rev. B*, **85**, 214516 (2012).
 - 42 Ding Hu *et al.*, unpublished polarized neutron scattering results on BaFe₂As_{1.4}P_{0.6}.
 - 43 See appended Supplementary Information for additional data and details on data analysis.
 - 44 Meng Wang, Chenglin Zhang, Xingye Lu, Guotai Tan, Huiqian Luo, Yu Song, Miaoyin Wang, Xiaotian Zhang, E.A. Goremychkin, T.G. Perring, T.A. Maier, Zhiping Yin, Kristjan Haule, Gabriel Kotliar, and Pengcheng Dai, *Nat. Commun.* **4**, 2874 (2013).
 - 45 Albert Furrer, Joël Mesot, and Thierry Strässle, *Neutron Scattering in Condensed Matter Physics* (World Scientific, 2009).
 - 46 J. T. Park, D. S. Inosov, A. Yaresko, S. Graser, D. L. Sun, Ph. Bourges, Y. Sidis, Yuan Li, J.-H. Kim, D. Haug, A. Ivanov, K. Hradil, A. Schneidewind, P. Link, E. Faulhaber, I. Glavatsky, C. T. Lin, B. Keimer, and V. Hinkov, *Phys. Rev. B* **82**, 134503 (2010).
 - 47 L. W. Harriger, H. Q. Luo, M. S. Liu, C. Frost, J. P. Hu, M. R. Norman, and Pengcheng Dai, *Phys. Rev. B* **84**, 054544 (2011).
 - 48 S. O. Diallo, D. K. Pratt, R. M. Fernandes, W. Tian, J. L. Zarestky, M. Lumsden, T. G. Perring, C. L. Broholm, N. Ni, S. L. Bud'ko, P. C. Canfield, H.-F. Li, D. Vaknin, A. Kreyssig, A. I. Goldman, and R. J. McQueeney, *Phys. Rev. B* **81**, 214407 (2010).
 - 49 M. M. Korshunov, Y. N. Togushova, I. Eremin, and P. J. Hirschfeld, *J. Supercond. Novel Magn.* **26**, 2873 (2013).
 - 50 S. Maiti, J. Knolle, I. Eremin, and A.V. Chubukov, *Phys. Rev. B* **84**, 144524 (2011).
 - 51 M. M. Korshunov and I. Eremin, *Phys. Rev. B* **78**, 140509(R) (2008).
 - 52 N. Qureshi, P. Steffens, D. Lamago, Y. Sidis, O. Sobolev, R. A. Ewings, L. Harnagea, S. Wurmehl, B. Büchner, and M. Braden, *Phys. Rev. B* **90**, 144503 (2014).
 - 53 P. Babkevich, B. Roessli, S. N. Gvasaliya, L.-P. Regnault, P. G. Freeman, E. Pomjakushina, K. Conder, and A. T. Boothroyd, *Phys. Rev. B* **83**, 180506 (2011).
 - 54 X. Lu, J. T. Park, R. Zhang, H. Luo, A. H. Nevidomskyy, Q. Si, and P. Dai, *Science* **345**, 657 (2014).
 - 55 Qiang Zhang, Rafael M. Fernandes, Jagat Lamsal, Jiaqiang Yan, Songxue Chi, Gregory S. Tucker, Daniel K. Pratt, Jeffrey W. Lynn, R. W. McCallum, Paul C. Canfield, Thomas A. Lograsso, Alan I. Goldman, David Vaknin, and Robert J. McQueeney, *Phys. Rev. Lett.* **114**, 057001 (2015).
 - 56 Wenliang Zhang, J. T. Park, Xingye Lu, Yuan Wei, Xiaoyan Ma, Lijie Hao, Pengcheng Dai, Zi Yang Meng, Yifeng Yang, Huiqian Luo, and Shiliang Li, *Phys. Rev. Lett.* **117**, 227003 (2016).
 - 57 A. E. Bohmer, F. Hardy, L. wang, T. wolf, P. Schweiss, and C. Meingast, *Nat. Commun.* **6**, 7911 (2015).
 - 58 Haoran Man, Xingye Lu, Justin S. Chen, Rui Zhang, Wenliang Zhang, Huiqian Luo, J. Kulda, A. Ivanov, T. Keller, Emilia Morosan, Qimiao Si, and Pengcheng Dai, *Phys. Rev. B* **92**, 134521 (2015).

Supplementary Information:

Determination of M_a , M_b and M_c

Using the method described in the supplementary of Ref. [1] and data for $\mathbf{Q} = (1, 0, L)$ with $L = 1$ and 3 ($L = 0$ and 2), we extracted M_a , M_b and M_c for the magnetic zone center (zone boundary along L) with odd (even) L . The data with $L = 3$ used in combination with the $L = 1$ data [Fig. 3(a)-(b)] to obtain M_a , M_b and M_c in Fig. 4(a)-(b) are shown here in Supplementary Fig. 1. In the analysis we ignored the differences of sample illumination volume and convolution with instrumental resolution between $L = 1$ and 3, and set the scale factor that accounts for these differences to be $r = 1$ [1]. In previous works [1–4] r is found to be close to unity in all cases and our results are qualitatively robust when r deviates slightly from 1.



Supplementary Figure 1: Temperature scans of σ_x^{SF} , σ_y^{SF} and σ_z^{SF} at $\mathbf{Q} = (1, 0, 3)$ with (a) $E = 3$ meV and (b) $E = 9$ meV.

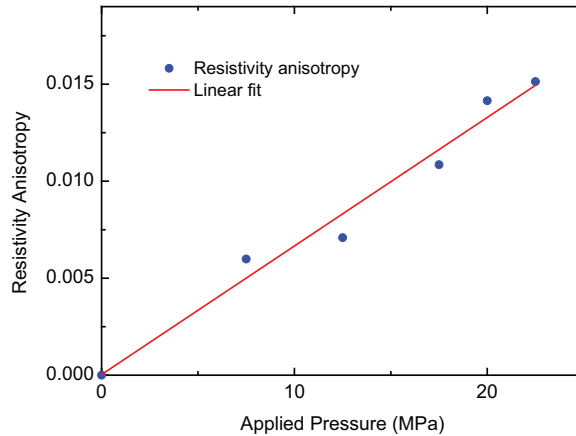
Measurement of resistivity anisotropy under uniaxial pressure

Previous measurements of resistivity anisotropy in $\text{Ba}_{1-x}\text{K}_x\text{Fe}_2\text{As}_2$ demonstrated that compared to their electron-doped counterparts, the hole-doped compounds have much smaller and reversed resistivity anisotropy [5, 6]. Near optimal doping resistivity anisotropy was found to disappear in $\text{Ba}_{0.66}\text{K}_{0.34}\text{Fe}_2\text{As}_2$ [6], however recent measurements revealed significant elasto-resistance in $\text{Ba}_{0.6}\text{K}_{0.4}\text{Fe}_2\text{As}_2$ [7]. To resolve this puzzling difference, we measured resistivity anisotropy on single crystals of $\text{Ba}_{0.67}\text{K}_{0.33}\text{Fe}_2\text{As}_2$ and $\text{BaFe}_{1.904}\text{Ni}_{0.096}\text{As}_2$ using the Montgomery method with a mechanical clamp that can vary the applied pressure *in-situ* as described in Ref. [8]. Prefactors due to samples not being perfect squares were corrected for at 200 K [8], where no/negligible resistivity anisotropy is present. Several nominal pressures were applied and the actual zero pressure is determined by performing a linear fit of the change in resistivity anisotropy as a function of nominal pressure. Measured resistivity anisotropy is then scaled to $P = 15$ MPa for both samples to allow for direct comparison under the same applied pressure. Resistivity anisotropy is linearly proportional to the applied pressure in the pressure range we studied, as shown in Supplementary Figure 2 for $\text{Ba}_{0.67}\text{K}_{0.33}\text{Fe}_2\text{As}_2$, similar to BaFe_2As_2 in which linear response persists up to 90 MPa in the paramagnetic state [8].

Our results are shown in Fig. 1(c), resistivity anisotropy with reversed sign is observed in optimally electron- and hole-doped BaFe_2As_2 samples. Significant anisotropy is seen in optimal-doped $\text{Ba}_{0.67}\text{K}_{0.33}\text{Fe}_2\text{As}_2$, in agreement with elasto-resistance measurements. The much smaller resistivity anisotropy in $\text{Ba}_{1-x}\text{K}_x\text{Fe}_2\text{As}_2$ and small applied pressure are likely causes of why it was not observed in previous work [6].

Anisotropy of the spin resonance with spin-orbit coupling

The spin excitations in the pnictides become anisotropic due to the spin-orbit coupling (SOC). At low energies, the excitations are peaked at the ordering vectors $\mathbf{Q}_1 = (\pi, 0)$ and $\mathbf{Q}_2 = (0, \pi)$. Therefore, we introduce two vector



Supplementary Figure 2: Resistivity anisotropy as a function of applied pressure. Data is obtained by combining measured points with $50 \leq T \leq 60$ K, a scaling factor used to normalize resistivity anisotropy to $P = 15$ MPa is obtained by a linear fit as shown.

order parameters, \mathbf{M}_1 and \mathbf{M}_2 . Following the theoretical results of Ref. [9], at sufficient hole-doping concentrations the c -axis becomes the easy axis, in agreement with experiments in Na-doped Ba122 [10]. Thus, the quadratic part of the free energy acquires the anisotropic contribution:

$$F(\mathbf{M}_1, \mathbf{M}_2) = \alpha_a (M_{1,a}^2 + M_{2,b}^2) + \alpha_b (M_{1,b}^2 + M_{2,a}^2) + \alpha_c (M_{1,c}^2 + M_{2,c}^2) \quad (\text{S1})$$

To simplify our analysis, hereafter we consider $\alpha_a = \alpha_b \equiv \alpha_{ab}$. According to Ref. [9], $\alpha_c < \alpha_{ab}$. In addition to the reorientation of the moments in the magnetic phase, the anisotropy of the spin excitations also affects the energy of the resonance mode in the s^{+-} superconducting (SC) phase. The spin resonance mode emerges as a spin-1 collective mode protected by the SC gap.

A full calculation of the spin resonance mode in the presence of spin-orbit coupling is beyond the scope of this paper (see Ref. [11]); here, we illustrate the effect of the spin anisotropy on the resonance mode using a semi-phenomenological approach. We consider a simple two band model containing one hole and one electron pocket. For simplicity, we assume perfect nesting – deviations from perfect nesting may shift the wave-vector of the resonance mode, as explained in Ref [12]. At low temperatures and deep inside the SC dome, we can treat the SC gap Δ as a constant. For a system without spin anisotropy, and within RPA, the resonance energy ω in the s^{+-} SC phase is given by the condition $\chi^{-1}(\mathbf{Q}, \omega) = U/2$, where U is the density-density interaction projected in the spin-spin channel, and $\chi^{-1}(\mathbf{Q}, \omega)$ is the isotropic non-interacting susceptibility inside the SC state. Performing the calculation, we find an implicit equation for ω :

$$\frac{1}{2UN_f} = \ln \frac{2\Lambda}{\Delta} + \frac{\omega}{\sqrt{(2\Delta)^2 - \omega^2}} \tan^{-1} \frac{\omega}{\sqrt{(2\Delta)^2 - \omega^2}}, \quad (\text{S2})$$

Here, Λ is the high energy cutoff and N_f is the density of states at the Fermi level. For small U , $\omega \lesssim 2\Delta$. As U increases, a magnetically ordered state appears inside the SC dome at the critical value $U^* = [2N_f \ln(\frac{2\Lambda}{\Delta})]^{-1}$, and the resonance mode vanishes.

Phenomenologically, the main effect of the spin anisotropy, as shown by Eq. (S1), is to shift the different components of the non-interacting spin susceptibility according to

$$\chi^{-1}(\mathbf{Q}, \omega) \rightarrow \chi_{ii}^{-1}(\mathbf{Q}, \omega) = \chi^{-1}(\mathbf{Q}, \omega) + \alpha_i \quad i = ab, c \quad (\text{S3})$$

As a result, the RPA condition $\chi_{ii}^{-1}(\mathbf{Q}, \omega) = U/2$ will give different resonance energies ω_i for different channels. Effectively, the critical value of the interaction U^* depends on the polarization channel. Since $\alpha_c < \alpha_{ab}$, we have $U_c^* < U_{ab}^*$. Physically, this means that for the same value of U , M_c is closer to its instability than M_a or M_b . Evaluation of ω_i then gives (assuming α_i small):

$$\frac{\omega_i}{\sqrt{(2\Delta)^2 - \omega_i^2}} \tan^{-1} \frac{\omega_i}{\sqrt{(2\Delta)^2 - \omega_i^2}} = \frac{1}{2N_f} \left(\frac{1}{U} - \frac{1}{U_i^*} \right), \quad (\text{S4})$$

Since $U_c^* < U_{ab}^*$, $\omega_c < \omega_{ab}$ in general, as shown in Fig. 4(c). The difference increases as U_c^* is approached, since at that point ω_c vanishes but ω_{ab} remains finite. For that figure, we used the parameters $U_{ab}^* N_f = 4/19$ and $U_c^* N_f = 0.2$.

-
- [1] Chenglin Zhang, Yu Song, L.-P. Regnault, Yixi Su, M. Enderle, J. Kulda, Guotai Tan, Zachary C. Sims, Takeshi Egami, Qimiao Si, and Pengcheng Dai, Phys. Rev. B **90**, 140502 (2014).
 - [2] Huiqian Luo, Meng Wang, Chenglin Zhang, Xingye Lu, Louis-Pierre Regnault, Rui Zhang, Shiliang Li, Jiangping Hu, and Pengcheng Dai, Phys. Rev. Lett. **111**, 107006 (2013).
 - [3] Chong Wang, Rui Zhang, Fa Wang, Huiqian Luo, L. P. Regnault, Pengcheng Dai, and Yuan Li, Phys. Rev. X **3**, 041036 (2013).
 - [4] Yu Song, Louis-Pierre Regnault, Chenglin Zhang, Guotai Tan, Scott V. Carr, Songxue Chi, A. D. Christianson, Tao Xiang, and Pengcheng Dai, Phys. Rev. B **88** 134512 (2013).
 - [5] J. J. Ying, X. F. Wang, T. Wu, Z. J. Xiang, R. H. Liu, Y. J. Yan, A. F. Wang, M. Zhang, G. J. Ye, P. Cheng, J. P. Hu, and X. H. Chen, Phys. Rev. Lett. **107**, 067001 (2011).
 - [6] E. C. Blomberg, M. A. Tanatar, R. M. Fernandes, I. I. Mazin, Bing Shen, Hai-Hu Wen, M. D. Johannes, J. Schmalian, and R. Prozorov, Nat. Commun. **4**, 1914 (2013).
 - [7] Hsueh-Hui Kuo, Jiun-Haw Chu, Johanna C. Palmstrom, Steven A. Kivelson, Ian R. Fisher, Science **352**, 958 (2016).
 - [8] Haoran Man, Xingye Lu, Justin S. Chen, Rui Zhang, Wenliang Zhang, Huiqian Luo, J. Kulda, A. Ivanov, T. Keller, Emilia Morosan, Qimiao Si, and Pengcheng Dai, Phys. Rev. B **92**, 134521 (2015).
 - [9] Morten H. Christensen, Jian Kang, Brian M. Andersen, Ilya Eremin, and Rafael M. Fernandes, Phys. Rev. B **92**, 214509 (2015).
 - [10] F. Waßer, A. Schneidewind, Y. Sidis, S. Wurmehl, S. Aswartham, B. Büchner, and M. Braden, Phys. Rev. B **91**, 060505 (2015).
 - [11] M. M. Korshunov, Y. N. Togushova, I. Eremin, and P. J. Hirschfeld, J. Supercond. Novel Magn. **26**, 2873 (2013).
 - [12] S. Maiti, J. Knolle, I. Eremin, and A.V. Chubukov, Phys. Rev. B **84**, 144524 (2011).

